Seismic entropic analysis based on magnitudes and time intervals

Eugenio E. Vogel,[1,2,*] D. Pastén,[3,†] and G. Saravia[4]
[1]*Departamento de Ciencias Físicas, Universidad de La Frontera, Casilla 54-D, Temuco 4811230, Chile*
[2]*CEDENNA, FINARQ, Universidad Central de Chile, Santiago 8330601, Chile*
[3]*Departamento de Física, Facultad de Ciencias, Universidad de Chile, Ñuñoa, Chile*
[4]*Los Eucaliptus 1189, Temuco 4812537, Chile*

(Received 14 July 2025; accepted 20 October 2026; published 2 November 2026)

Usually, seismic analyses are based on magnitudes which are obtained from models based on the energy released by each earthquake. The present approach supplements this description by including the intervals between consecutive events. This is justified by arguments coming from fundamental physics: energy and time are canonical variables, so they offer complementary and equally acceptable descriptions of the same phenomenon. We then apply both schemes to four seismic zones along the coast of the Pacific Ocean (part of the "circle of fire") surrounding the following major earthquakes: $Mw8.2$ in Alaska (2021), $Mw7.1$ in California (2019), $Mw8.2$ in Iquique (2014), and $Mw8.8$ in Maule (2010). Following a basic statistical characterization, we applied mutability and diversity analyses—two information theory techniques related to Shannon entropy—to the magnitude and interval sequences. The analysis of the interval sequences provides an accurate description of the seismic activity. Magnitude and intervals present opposite variations in the dynamical analyses, thus offering complementary descriptions of the same phenomenon. However, the results for intervals render a more direct interpretation of the seismic sequence.

DOI: 10.1103/xj32-b6tj

I. INTRODUCTION AND BACKGROUND

The seismic activity of the planet has always been a source of new questions and, in recent years, new ways of addressing them have emerged. Among these is entropy, a statistical physics tool that researchers are increasingly using in the study of seismicity, whether it is the classic Shannon entropy or the nonextensive Tsallis entropy [1–9].

Seismographs record several parameters with each earthquake, which are input to algorithms that provide quantitative information. The most usual characteristics are magnitude, epicenter (latitude and longitude), depth, initial time, duration, and nonquantitative characteristics. The property most frequently reported is the magnitude, which provides information about the strength of the telluric phenomenon.

In reality, there is no unique way to find the magnitude and other features of an earthquake, as there are different ways to achieve the corresponding values of the parameters. The following aspects affect the reported magnitude. (1) The value is calculated with the information provided by the networks of connected stations, which are heterogeneous in manufacture and antiquity. (2) This information is processed according to algorithms used by different seismological centers. (3) The value is being updated as the successive information from the stations arrives at the seismological center. (4) The final value reported depends on the network of stations. (5) In the case of magnitudes, definitions have evolved. (6) Most of the parameters depend on the model of the seismic wave propagation.

So, it is not surprising that an earthquake can be reported with different characteristics in catalogs from different seismological centers. Thus, for example, let us consider the earthquake of 2012.09.19 (YYYY.MM.DD format), occurring in Mexico. The Servicio Sismológico Nacional of Mexico (SSNM) reported its beginning time at 18:05:09 (HH:MM:SS format) local time, at a depth of 12.1 km, with coordinates −103.27 latitude and 18.24 longitude, with a magnitude of 7.7 [10]. The United States Geological Survey (USGS) [11] reports the same earthquake beginning on 18.05.08 local time, at a depth of 26.9 km, with coordinates −102.96 latitude and 26.94 longitude, and with a magnitude of 7.6. The less significant difference is one second for the beginning of the earthquake, but all other differences are notorious. Actually, the difference in magnitude of decimal points is large because of the logarithmic scale used to determine this parameter. This is just one example, but differences in parameters occur when comparing catalogs [11].

From the previous paragraph, a question immediately follows: which parameter has less uncertainty? The immediate answer is the time at the beginning of an earthquake. This is even more so if seconds are left out, as will be done in this work. Then, the time and time intervals are essentially exact up to one minute.

*Contact author: eugenio.vogel@ufrontera.cl
†Contact author: denissepasten@uchile.cl

Published by the American Physical Society under the terms of the Creative Commons Attribution 4.0 International license. Further distribution of this work must maintain attribution to the author(s) and the published article's title, journal citation, and DOI.

So, in the rest of this analysis, we will carry out parallel calculations based on magnitudes and time intervals of a set of seisms with characteristics extracted from catalogs that we will quote. For the reasons already discussed above, we will stick to one catalog per region under study without combining data from different catalogs.

The main quantitative approach uses entropy related functions, such as mutability and diversity, to be defined in Sec. IV. They will apply to sequences of magnitudes and time intervals for seisms before and after the following major earthquakes along a portion of the "circle of fire" lying on the east side of the Pacific Ocean. Subduction processes primarily dominate seismic activity along the Pacific coast of the American continent, although it varies. In North America, there is an interaction between the oceanic Pacific plate that submerges under the North American plate, forming the Aleutian Trench [12–17]. In Central America, we find a complex tectonic setting that includes the interaction between the North American, Cocos, Caribbean, and Nazca plates. This interaction produces the Mid-American trench with high seismic activity in the area [18–20]. Finally, further south, the interaction between the Nazca plate and the South American plate has led to a destructive interaction that has produced major earthquakes in the past 15 years [21–24]. The seismic richness of this area motivates us to conduct a comparative analysis of the aforementioned entropic functions for four major earthquakes that occurred on the west coast of the American continent. From North to South, the major seismic events of the present century include (i) the Mw 8.2 earthquake in Alaska (USA) in 2021 [11], (ii) the Mw 7.1 earthquake in California (USA) in 2019 [11], (iii) the Mw 8.2 earthquake in Iquique (Chile) in 2014 [25], and (iv) the Mw 8.8 earthquake in Maule (Chile) in 2010 [26]. Modern equipment registered all these major earthquakes during the 21st century; these earthquakes, with magnitudes over 7.0, originated from the subduction of oceanic plates under continental plates.

We can summarize the main innovations of this article as follows. The analysis of the seismic sequence equally considers both seisms' magnitudes and time intervals between consecutive seisms (referred to as *intervals* from now on). Introducing the concept of *latency* (logarithm of the interval between consecutive events) allows comparison with the magnitude of the seisms (related to the logarithm of the relaxed energy). To the analysis by mutability of earthquake sequences, we add here results of *diversity*. Results obtained from the intervals show details that compete with those contributed by magnitudes. Our purpose is to add different approaches to those already existing in seismology, mainly based on entropic functions like diversity and mutability. The latter carries information on the dynamics of the system as explained below. In Appendix A we compare results obtained using these functions to those obtained by Shannon entropy. This study uses data from four different seismic regions along the "ring of fire," enabling a generalizable approach.

This paper is organized in the following way. The next section recollects the theoretical justifications for dealing with magnitudes and intervals as parallel descriptions of the same phenomenon. The third section covers data sources and organization. Section IV reviews the definitions of both mutability and diversity. Section V dynamically presents our results, using composed graphs to illustrate the key features used in the discussions. The sixth section summarizes the conclusions.

II. THEORETICAL CONSIDERATIONS

Theoretical physics establishes relationships between canonical variables. Thus, for instance, in classical mechanics, the Poisson brackets relate position and momentum in the following way [27]:

$$\{x_k, p_l\} = -\{p_k, x_l\} = \delta_{k,l}, \tag{1}$$

where k and l identify the Cartesian axes and $\delta_{k,l}$ is the well-known Kronecker delta. In this way, the position along a direction and the momentum along the same direction are related.

This concept is extended to quantum mechanics in the form of commutators [28], namely

$$[x_k, p_l] = -[p_k, x_l] = i\hbar\, \delta_{k,l}, \tag{2}$$

where i is the imaginary unit and $\hbar$ is the Planck constant.

The relationships between pairs of canonical variables are also present in Heisenberg´s uncertainty principle [28]:

$$\Delta x_k \Delta p_l \geqslant \frac{\hbar}{2}\, \delta_{k,l}, \tag{3}$$

where Δx_k is the uncertainty in the position along the k component, while Δp_l is the uncertainty in the momentum along the l component. So when the position along a direction is very well known, the corresponding momentum component is not well known and vice versa.

Similar relationships hold for the canonical scalar variables energy E and time t [28]. That is,

$$\Delta E\, \Delta t \geqslant \frac{\hbar}{2}. \tag{4}$$

A wave of any nature in one dimension is generally expressed as

$$y(x, t) = f(kx - \omega t), \tag{5}$$

where k is the wave vector that can be associated in quantum mechanics with the linear momentum p by the relationship $p = \hbar k$; similarly, the frequency ω can be associated with the energy E by $E = \hbar\omega$. So, again, here, the canonical variables play complementary roles.

In the present article, we can formally treat energy and time as canonical variables in a classical way. On one hand, large seisms (large magnitudes) are usually preceded by foreshock seisms of moderate magnitude (less than 4.0 say), while they give rise to a sequence of aftershock seisms of all magnitudes (including earthquakes of magnitude 5 or larger). On the other hand, seisms in the foreshock regime are scarce leading to large intervals (weeks or even months), while they occur very often in the aftershock regime (with intervals of hours or minutes). This clearly tells of complementary behaviors of magnitudes and intervals.

Despite differences in the definitions and calculations of seismic magnitudes, these relate to the logarithms of the energy dissipated in the corresponding earthquakes. Therefore, let us consider this energy ΔE and the time interval

TABLE I. Four large earthquakes studied in this work, ordered from North to South. The columns bear the following information: (1) geographical name; (2) magnitude (M); (3) date (YYYY.MM.DD); (4) latitude; (5) longitude; (6) depth (D) in km; (7) number of seisms originally gathered in the data extraction described in the text.

Place	M	Date	Lat.	Long.	D	No.
Alaska	8.2	2021.07.29	55.36	−157.89	35.0	10255
Calif.	7.1	2019.07.06	35.77	−117.60	8.0	15177
Iquique	8.1	2014.04.01	−19.59	−70.94	19.91	14210
Maule	8.8	2010.04.01	−36.26	−73.19	6.95	7730

Δt between successive events as interconnected in a manner similar to canonical variables. Then, we can formally try to describe the same seismic phenomenon by energy or intervals, which could provide complementary descriptions of the phenomenon. Our approach uses this as its basis and we will present results based on both magnitude (related to the logarithm of ΔE), intervals between consecutive seisms τ, and what we will call *latency* (the logarithm of τ), which we will properly define below.

III. SYSTEMS UNDER STUDY AND BASIC STATISTICAL METHODS

In the first part of this section, we review the seismic catalogs, data extraction, and data organization. The second subsection does basic statistics with the magnitude sequence. The next subsection deals with the intervals. The last subsection mixes the analysis using both magnitudes and intervals.

A. Seismic data

We defined a curved quadrilateral (rectangle) on the Earth's globe around each of the earthquakes listed in Table I, spanning two degrees north, south, east, and west. We extracted all seisms up to 60 km deep, before and after the corresponding large earthquake, from the catalog stated in the following summary.

Alaska seisms. The USGS catalog is used [11]. All the seisms with latitudes between 53.36 and 57.36 and longitudes between −159.89 and −155.89, from 2010.01.01 to 2024.12.31, are extracted. This means 19 576 earthquakes, three of which are over magnitude 7.0. The sequence of all these magnitudes is plotted in Fig. 1, upper left.

California seisms. The USGS catalog is used [11]. All seisms with latitude between 33.77 and 37.77 and longitude between −119.60 and −115.60, from 2010.01.01 and 2024.12.31, are extracted. Just one earthquake with a magnitude of 7.0 is present here. This means a total of 151 788 seisms. The sequence of these magnitudes is plotted in Fig. 1, upper right.

Iquique seisms. The IPOC catalog is used [25]. All seisms with latitude between −17.57 and −21.57 and longitude between −68.91 and −72.91, from 2007.01.01 and 2014.12.31, are extracted. Unfortunately, no recent updates to this catalog are available. This means 14 211 seisms, two very consecutive earthquakes with a magnitude over 7.0, are in this set. The sequence of these magnitudes is plotted in Fig. 1, bottom left.

Maule seisms. The CSN catalog is used [26]. All seisms with latitude between −34.29 and −38.29, and longitude between −71.24 and −75.24, from 2005.01.01 and 2021.12.31, are extracted. No recent updates to this catalog are available. This means 7718 seisms. Just one earthquake with a magni-

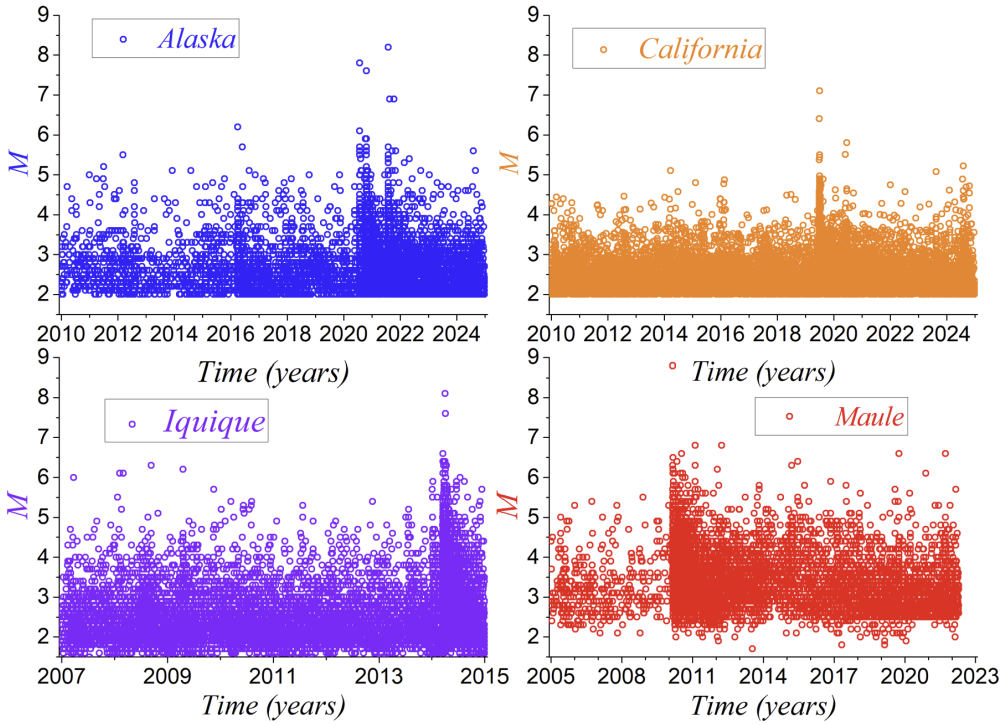


FIG. 1. Magnitude versus time of the earthquakes corresponding to each of the four zones around the four earthquakes listed in Table I: Alaska, California, Iquique, and Maule.

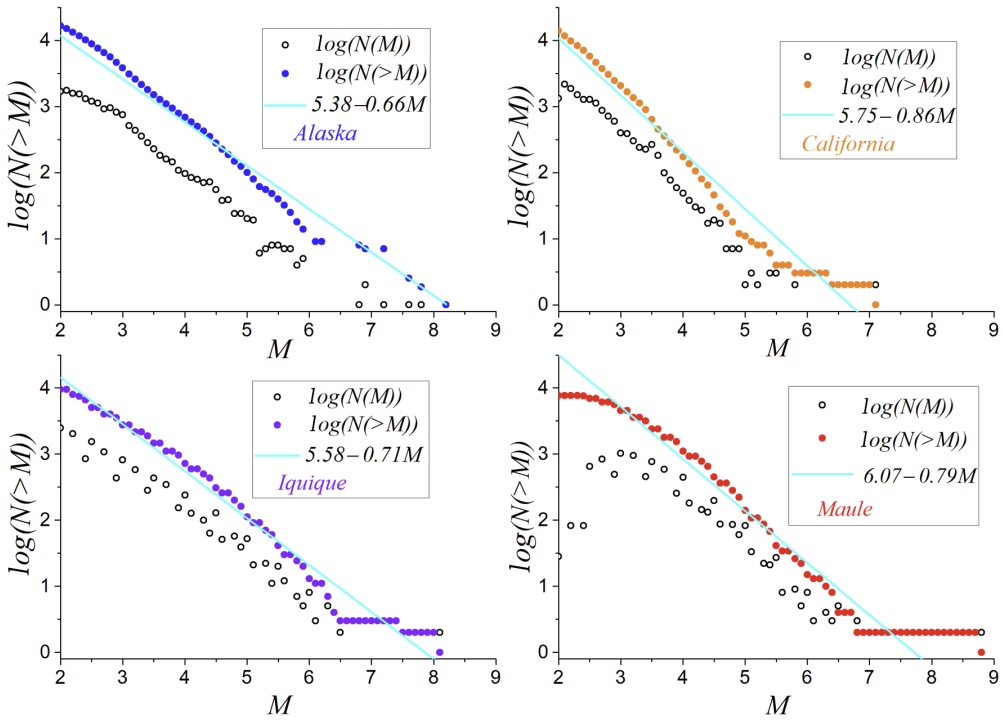


FIG. 2. Gutenberg-Richter analysis on magnitude M for the four zones under study: Alaska, California, Iquique, and Maule. In cyan the straight line corresponding to the linear fit given by Eq. (6).

tude over 7.0 is present here, corresponding to the largest one included in this work with a magnitude of 8.8. The sequence of these magnitudes is plotted in Fig. 1, bottom right.

We adopt a color code to quickly identify results for each region: blue for Alaska, orange for California, violet for Iquique, and red for Maule. This scheme will be used for all remaining graphs.

B. Magnitudes

As shown in Fig. 1, the information density varies across regions, mainly due to the catalog used for data extraction. The Maule region has the lowest seismic density of the four. In fact, we visited catalogs from other regions that were discarded due to their lack of low-magnitude seisms, thereby hampering the statistical analysis. Unlike controlled laboratory experiments, in this case, we have to handle the available data, bearing in mind the differences among the sources.

However, the four magnitude graphs have some common features and also some specific characteristics. (i) The density of earthquakes is lower before the large seisms. (ii) The density of earthquakes is larger immediately after a large earthquake in what is usually called the aftershock regime. (iii) Alaska has the largest number of earthquakes with magnitude over 7.0, while Maule has only one, which is the largest of all those considered here and the sixth all over the world since there is an instrumental record [11]. (iv) We clearly appreciate linked seisms as columns associated with one seism of magnitude 6 or higher (see, for instance, 2016 in Alaska, 2020 in California, 2008 in Iquique, and 2012 in Maule).

The ordinate in each panel immediately renders the strongest earthquakes in the corresponding region. We will pay special attention to earthquakes with a magnitude of 7.0 or higher. We observe that a large amount of seismic activity follows each such earthquake, corresponding to the aftershock regime. This contrasts with the foreshock regime, which shows fewer earthquakes. Before the magnitude 7.0 earthquakes in Alaska and Iquique, lower seismic activity occurs. The opposite is not always true: the scarcity of seisms is not necessarily an announcement of future vigorous activity (see, for instance, Alaska in 2013 or Iquique in 2011). However, the seismic activity is a sign that can be of interest.

An initial statistical analysis usually performed on seismic data is the Gutenberg-Richter plot as presented in Fig. 2 for the four regions under study. The lower curves correspond to the logarithm of the corresponding histograms $f(M)$, corresponding to the frequency of each magnitude. The upper curves give the logarithm of the accumulated number of earthquakes with a magnitude greater than the value M. This curve is characterized by a linear descent in the number of seisms as M grows. The Gutenberg-Richter law reveals the self-similar nature of earthquake occurrence, indicated through the proportion of small and large seismic events (a low b value shows a major number of large events). The straight lines (in cyan) in Fig. 6 follow least-square fits on that portion of the curves according to the law:

$$\log(N(>M)) = a - bM, \tag{6}$$

where M is the magnitude in each plot, a is the intercept on the ordinate axis, and b is the corresponding slope. The equation of each inset shows the following b values: 0.66 for Alaska, 0.86 for California, 0.71 for Iquique, and 0.79 for Maule [1,2,19,29–35]. We obtain different b values for the four different tectonic environments. Commonly, the b value is close to 1.0, but it varies across seismic zones. Based on Schorlemmer [35], small values of b are related to high

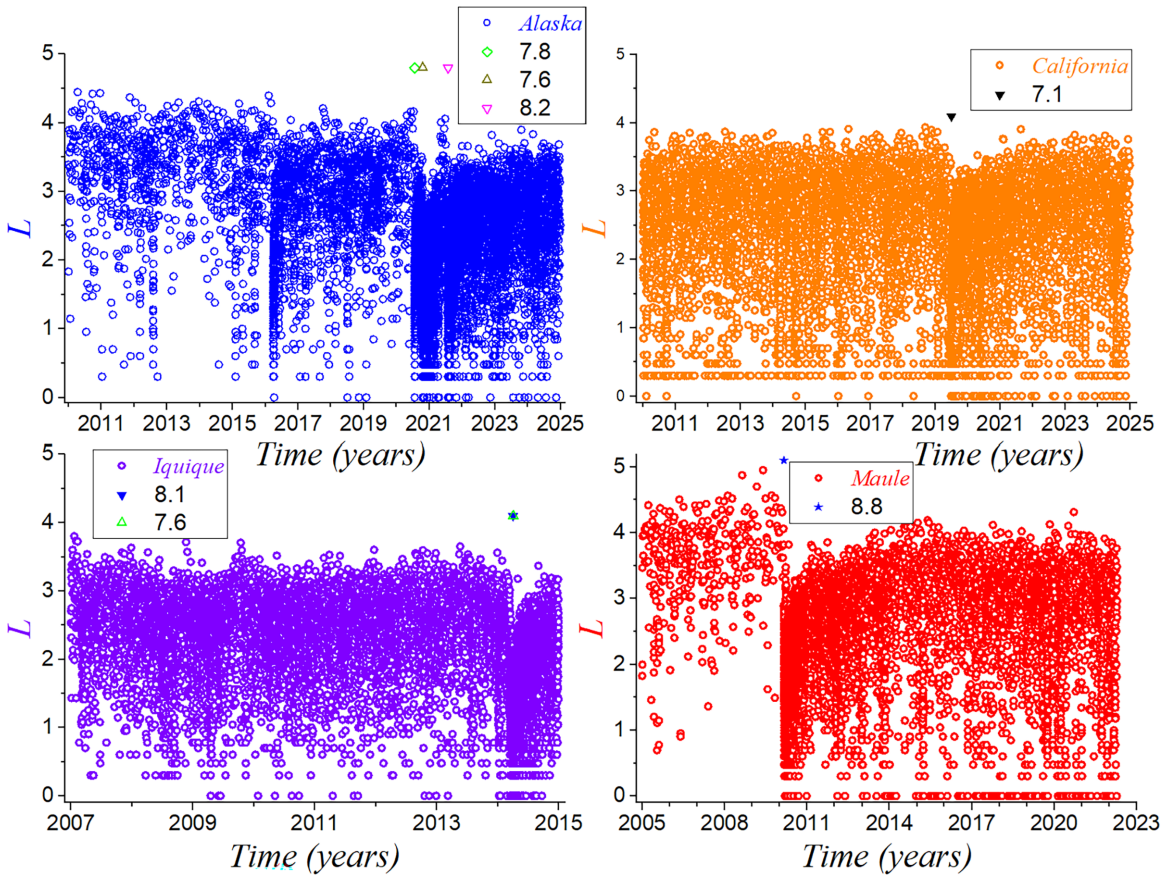


FIG. 3. Latency versus time of the earthquakes corresponding to each of the four zones around the four earthquakes listed in Table I: Alaska, California, Iquique, and Maule.

stress, while larger values (close to 1.0) are associated with low stress in the zone. In this work, we use four different tectonic environments, as shown in Fig. 2, to apply mutability and diversity.

C. Intervals

Usually, catalogs give the initial time of the earthquake in columns using the following code: YY/MM/DD/HH/mm/SS, corresponding to year, month, day, hour, minute, and second, respectively. Following the discussion in the Introduction, we leave completely out of consideration the seconds, creating a new column with the actual time $t = t_i$ of the occurrence of the ith seism expressed in minutes. Then, we add a column with the intervals τ as the difference between consecutive events, namely, $\tau_i = t_i - t_{i-1}$. For completeness we define $\tau_1 = 0$. Such intervals can go from zero minutes up to five orders of magnitude in the data we handled.

In each case, the extracted data led to two different vector files. File A contains the sequence of magnitudes M and file B contains the sequence of intervals τ between consecutive events. Because the intervals span five digits, we achieve better comparison with magnitudes using their logarithm, which we call *latency* L and store in a third vector file. Namely,

$$L(t) = \log(\tau(t)). \tag{7}$$

Figure 3 gives the latency as a function of time, $L(t)$, in a way similar to the one presented in Fig. 1 for magnitudes. At first sight, we see downward columns correlate with large earthquakes, whose magnitudes appear in each graph's inset. The upper left panel presents the latency of Alaska, revealing the columns for the activity of 2020 and 2021. But the activity for the 2016 earthquake ($Mw6.6$) is better shown for latency than for magnitude. The latency plot shows a notorious activity during 2012, undetected in the magnitude figure. The other three panels also show similar columns of concatenated seismic activity. After a large earthquake, as shown by special symbols defined in the insets, the latency decreases, which is a manifestation of the significant activity during the aftershock regime.

Figure 1 and Fig. 3 provide complementary information and it is possible to appreciate that latency presents more details than magnitude. Thus, although the number of points is the same in both figures, the magnitude curves accumulate them for the lower values, while the latency curves present them relatively spread. Latency also allows a first characterization of the regions according to their values before the first large earthquake: the average maximum level was nearly 4.2 for Alaska, 3.9 for California, 3.8 for Iquique, and 4.9 for Maule. This tells of the different dynamics of the subduction process in the underground of each region. As the large earthquake unclogs the subduction process, the plates can flow through smaller quakes and the latency (intervals) decreases, as shown in the four panels of Fig. 3. Symbols on top, defined in the respective insets, indicate the times

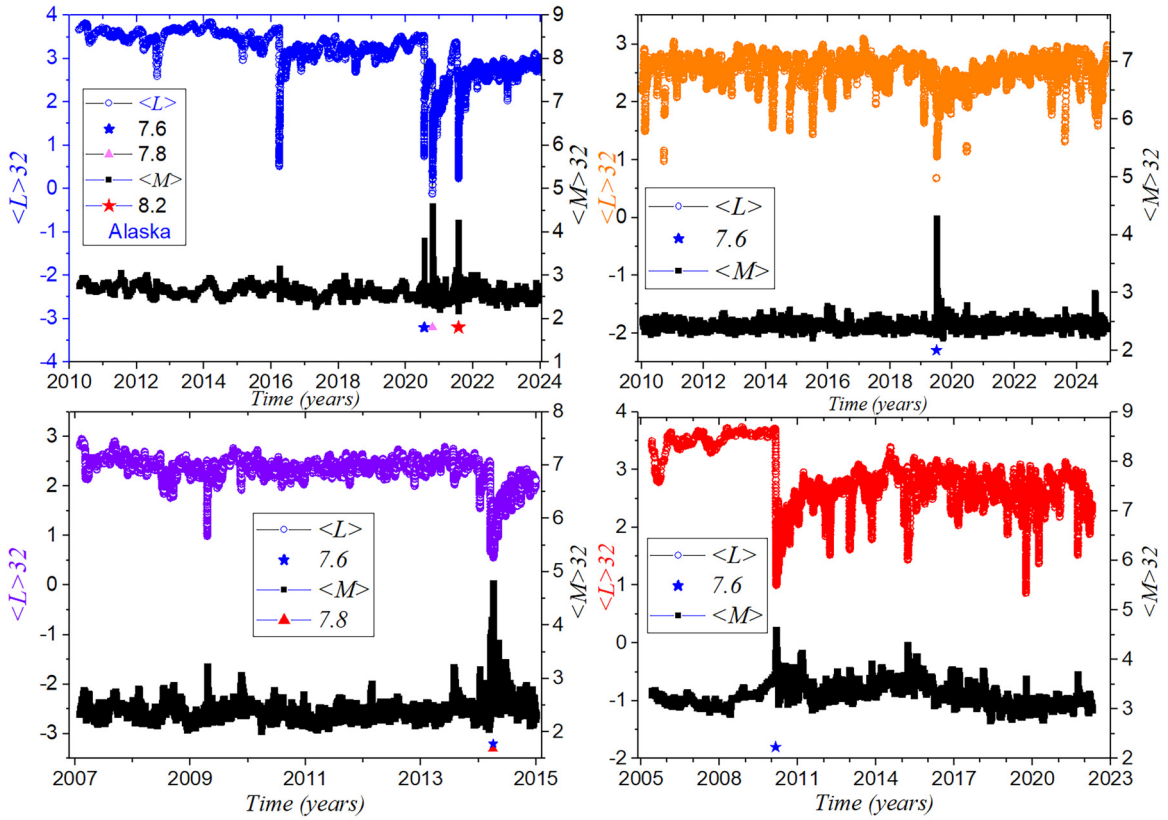


FIG. 4. Dynamical average magnitude $\langle M \rangle$ ($W = 32$) and dynamical average of latency $\langle L \rangle$ ($W = 32$) for Alaska, California, Iquique, and Maule. Vertical spans are similar within each plot for comparison.

of the largest earthquakes. It is possible to recognize the timing of other significant earthquakes below magnitude 7.0, corroborated by the data files. The 6.2 Alaska earthquake of April 2, 2016, demonstrates this, appearing in the upper left panel as a vertical alignment of blue points at the start of 2016. The Iquique data (lower left panel) shows a similar situation during 2008 because of a 6.3 magnitude earthquake on 2008.09.10.

From the previously discussed two figures, it follows that the seismicity of California differs from that of Alaska and Iquique: magnitudes are lower, while intervals are shorter. Alternatively, the reduced seismicity reported in the Maule zone (especially for low magnitudes; see Fig. 1, lower panel) prohibits a comparative analysis.

D. Magnitude and latency

The logarithm of the energy released by the corresponding earthquake relates to the magnitudes and we defined latency as the logarithm of the intervals τ using Eq. (7). They both span similar ranges, so it is possible to plot them together to appreciate their common features and differences.

Figure 4 presents the dynamical average value for time windows of 32 events, overlapping in one event, both for magnitudes (lower curves) and intervals (upper curves) for the four regions considered here. Special symbols show the timing of earthquakes above magnitude 7.0. Latency curves present more texture than those for magnitude, which remain flatter. Despite this important difference, both curves clearly respond to the largest seism in each region: magnitude curves as ascending peaks and latency curves as descending or inverse peaks at the same time.

Notice that the vertical span is nearly the same for magnitude and latency within each panel. This allows a comparison of the sensitivity or response of each parameter. Apart from the seisms above 7.0, latency presents a stronger response for intermediate seisms. Consider, for example, the seisms in 2026 for Alaska, 2023 for California, 2009 for Iquique, and 2019 for Maule. The general contrast for the latency curves is also larger than the corresponding one for magnitudes.

The same order and colors used in previous figures are used, except for the curves of $\langle M \rangle$, which are all black to contrast with the $\langle L \rangle$ curves, which are colored. Special symbols at the bottom of the figures mark the times of the largest seisms; the insets define them.

Several comments are in order regarding Fig. 4. First, $\langle M \rangle$ curves are flatter than $\langle L \rangle$ curves, presenting fewer slope variations. Second, $\langle L \rangle$ curves present more variations than $\langle M \rangle$ curves. Third, both curves reveal upwards ($\langle M \rangle$) and downwards ($\langle L \rangle$) "needles" coinciding with important earthquakes. Fourth, $\langle L \rangle$ curves show better the occurrence of intermediate seisms than $\langle M \rangle$ curves; see, for instance, Alaska 2016, Iquique 2009, or Maule 2019. Fifth, we detect no clear premonitory signs days or weeks before the large earthquakes.

IV. INFORMATION THEORY

The Shannon entropy of the state distribution represented in the file directly relates to the information content of a vector

file storing the evolution of an observable [36,37]. Mutability, an extension of Shannon entropy that reflects the dynamical properties of the sequence, was later introduced [38,39]. This entropy-based function has seen use in various fields for over a decade. To avoid repetitions, we summarize recent references applying this function precisely to seismicity: comparing it with Shannon entropy [6,39] and Tsallis entropy [40,41]. We introduced a second parameter derived from information theory, diversity, a decade ago [42], but then used mutability because of its dynamic characteristics. We invite readers interested in the entropic implications of this work to check the previously quoted articles and related references.

In the present article, we will use both mutability and diversity to discuss the behavior of the magnitude and interval sequences of the four regions under study. We begin by recovering the definitions of mutability and diversity, followed by an example based on a segment of real seismic data to illustrate these definitions.

A. Mutability and diversity

Let $Q(t)$ be a sequence in time t of R registers (measurements) of any parameter of interest. The weight in bytes of the vector file holding this information is $w(Q,R,t)$. Let R^* be the different values among the R previous registers. Then, we generate a second file with R^* rows that begins with the different values in sequential order of their appearance. To the right of each register, a coded method similar to data compressors provides the subsequent positions of the register's appearance (an example will describe this below). The weight in bytes of this second file is denoted by $w^*(q,R)$. Note that this compressed file omits the time t. Then mutability is simply given by [6,43–47]

$$\zeta(Q,R,t)=\frac{w^*(Q,R)}{w(Q,R,t)}. \tag{8}$$

Diversity bears an even simpler definition [42], namely

$$\delta(Q,R,t)=\frac{R^*}{R(Q,t)}. \tag{9}$$

It has been recently found that diversity can be expressed as a functional of entropies [48].

To better illustrate previous definitions we make use of Table II. The first column enumerates the sequence of $R=32$ measurements stored in the second column labeled M. The third column lists the different values within the previous column in the order they appear. The fourth column stores the positions of the repeated values in a coded way. This task can be achieved in different ways, we do it by means of the data recognizer WLZIP which works in the following way: we scan the second column from top to bottom; we write each new value in the third column, followed in the fourth column by its distance from the first value (origin) in column 2. Subsequent occurrences of a value are denoted in the fourth column by its distance to the last appearance in column 2. We denote a value repeating r times by appending "$,r$" after the last distance. In this way, each value of the parameter appears only once in the third column. The relative distances between repetitions do not require large numbers. The generated map keeps records of the dynamics of the data sequence and it allows one to recover the original file without losing information. The logic of each single step algorithm in previous protocol is illustrated in a flowchart given in Appendix B, where we also offer the program WLZIP to the interested readers.

TABLE II. Magnitudes and intervals for a sequence of $R=32$ consecutive seisms from the Alaska set during 2016. The first column is just a sequential index; column 2 lists the corresponding magnitudes; columns 3 and 4 store the map produced by wlzip. Frequencies for the values in the third column are collected in the fifth column. The sixth column is a spacer. Column 7 lists the corresponding intervals τ, followed by the corresponding map in columns 8 and 9. The last two rows give the values of mutability and diversity of magnitudes and intervals according to Eqs. (8) and (9).

i	M		Map (M)	f	τ		Map (τ)
1	2.2	2.2	0 3	2	00285	00285	0
2	2.1	2.1	1 5	2	04516	04516	1
3	2.4	2.4	2 7 2	3	01162	01162	2
4	2.2	3.7	4	1	02963	02963	3
5	3.7	2.6	5 23	2	03228	03228	4
6	2.6	3.3	7 9 4	3	19211	19211	5
7	2.1	3.2	8	1	00765	00765	6
8	3.3	2.3	10 13	2	06365	06365	7
9	3.2	6.2	12	1	07444	07444	8
10	2.4	4.1	13	1	10359	10359	9
11	2.3	3.5	14	1	01808	01808	10
12	2.4	3.4	15 7	2	03438	03438	11
13	6.2	3.1	17 8	2	07473	07473	12
14	4.1	4.4	18	1	00002	00002	13,2 2,2 5,2 2,4
15	3.5	2.8	19 11	2	00002	00001	15 3 2
16	3.4	3.0	21 5,2 2 2	5	00001	00005	19 2
17	3.3				00002	00007	29
18	3.1				00002	00004	30
19	4.4				00001	00006	31
20	2.8				00005		
21	3.3				00001		
22	3.0				00005		
23	3.4				00002		
24	2.3				00002		
25	3.8				00004		
26	3.1				00002		
27	3.0				00002		
28	3.0				00002		
29	2.6				00002		
30	3.0				00007		
31	2.8				00004		
32	3.0				00006		
ζ			1.0125				0.9063
δ			0.5000				05938

In this paragraph we test the previous steps to build the map corresponding to the magnitudes in the second column of Table II (the map of the column labeled τ for the intervals is built similarly). Readers not interested in these details may skip this paragraph. Integers in the first column sequentially label the events. The first value of the parameter Q in the second column is 2.2, so we write it in the third column, continuing to the fourth column where we write 0, which is its distance to the first value in column 2 (distance to itself in this case). Then we go back to the next value in the second

column, namely 2.1, which is a new value, so we write it in the third column and in the fourth column its distance, 1, to the origin of the second column. Similar situation with the value 2.4, with its distance 2 to the origin of column 2. But when we go to the fourth register in column 2, we find an already known value, 2.2; then we go back to the row with this value in the third column and add 3 to the right in the fourth column, which is its distance to the last time 2.2 showed in the second column. The process continues like this up to line 22, when the value 3.0 appears for the first time, so we write it down in the third column and the distance 21 in the fourth column. Then, the value 3.0 appears in row 27, at a distance of 5 from the last appearance, so we write 5 in the fourth column. Since 3.0 repeats itself in the next row, we add a comma to the last distance and write 2 (the number of consecutive repetitions). Then the value 3.0 appears a single time two positions below and again a single time two positions from the last show.

The weight in bytes of the second column is w while the weight in bytes of the third and fourth columns together is w^*. Then the mutability for the observable Q is given by Eq. (8). In the last two rows of Table II we give the mutability and diversity values for the examples.

B. Application to magnitudes and intervals

The previous presentation is general and it can apply to any observable. However, Table II represents real seismic data corresponding to a segment of the extracted data for Alaska, including the 6.2 earthquake of 2016. So in column 2 Q corresponds to the magnitudes M of the corresponding sequence of seisms; columns 3 and 4 are for the map of the magnitudes produced by wlzip; column five is for the frequencies of the magnitudes. The mutability and diversity for magnitudes can be obtained from columns two and the combination of columns three and four.

After the sixth narrow column for spacing in Table II, we find the seventh column with the sequence of intervals τ between consecutive seisms. Notice that all entries have five digits to facilitate recognition (a blank is not a digit). As we did for the magnitudes, the eighth and ninth columns make the map of the seventh column by using WLZIP . One can readily calculate mutability and diversity corresponding to the intervals using the information in the seventh and the combination of the eighth and ninth columns.

The row labeled ζ gives the values of the mutability for magnitudes and at intervals using Eq. (8). Similarly, the row labeled δ gives the values of the diversity for magnitudes and at intervals by Eq. (9).

The fourth column readily provides the frequency $f(i)$ for the value given in the third column. These frequencies f_i give the probability p_i for the ith value in column 3:

$$p_i = \frac{f_i}{R}, \tag{10}$$

where R is the number of records in the second column. The larger the sampling, the more representative this probability is. With these probabilities, we can get the Shannon entropy as

$$H = -\sum_i p_i \ln(p_i). \tag{11}$$

We include this expression just to show the connection between Shannon entropy and mutability. The frequencies generated by WLZIP and stored in the ninth column yield the Shannon entropy for the τ sequence. However, we omit an additional column listing those frequencies, as we already illustrated this process for magnitudes, and we will not calculate Shannon entropy this time.

V. RESULTS AND DISCUSSION

We now present results on mutability and diversity for the magnitude series and intervals τ. The reason to prefer τ over L here is the larger number of significant digits of the former.

The results are presented dynamically using overlapping time windows of R consecutive events. The overlap is just one event. We use $R = 256$ as it is justified in Appendix C. This number of records was already used in previous seismological studies [41], which can allow for comparison. Smaller windows yield noisier curves, while larger windows lose anticipation.

The analysis by entropic functions begins with Fig. 5, presenting the dynamical mutability on magnitude sequences. The real time for the result is the time of the last seism of each time window. Special symbols at the top denote important earthquakes and the insets define them.It is clear that mutability on magnitudes maximizes at the time of a large seism, since the large quake and its important aftershock response break the previous monotony. However, the different zones differ in their tendencies. In Alaska, before large seismic events, the average ζ slowly decreases; however, mutability returns to its previous values afterward. California shows no significant overall variations. With Iquique, the mutability goes through a broad minimum near 2011-2012, a couple of years before the major quakes. Unfortunately, not enough seisms are available in the IPOC catalog prior to the 2010 earthquake to discuss the foreshock process in Maule. On the other hand, the absolute minimum observed at the beginning of 2021 during the aftershock response differs from the aftershock regime in the other regions and invites watching the future evolution of this area.

Absolute values of mutability are different among the zones. Iquique reached the maximum mutability of about 0.72, showing a wide range of magnitudes following the 8.1 earthquake. California exhibits a minimum of about 0.53, consistent with the region's lower seismic activity. Probably, this tells about the underground conditions prevailing that trigger the quakes, but this does not allow for comparison among the different zones. Figure 6 presents the results of mutability based on intervals (τ) sequences for the four zones using the same previous scheme. The major earthquakes are clearly marked as downward "needles" at the corresponding times. However, more texture is observed in these curves as compared to those of the previous figure. Even for California, where no obvious patterns were possible in Fig. 5, we now observe secondary seisms in 2014, in 2020, and in 2024. The vertical span on all plots of Fig. 6, covering an order of magnitude, allows for better characterization of the different regimes in each zone. Another interesting feature of these curves is the narrowness of the needles, perfectly marking the most important earthquakes.

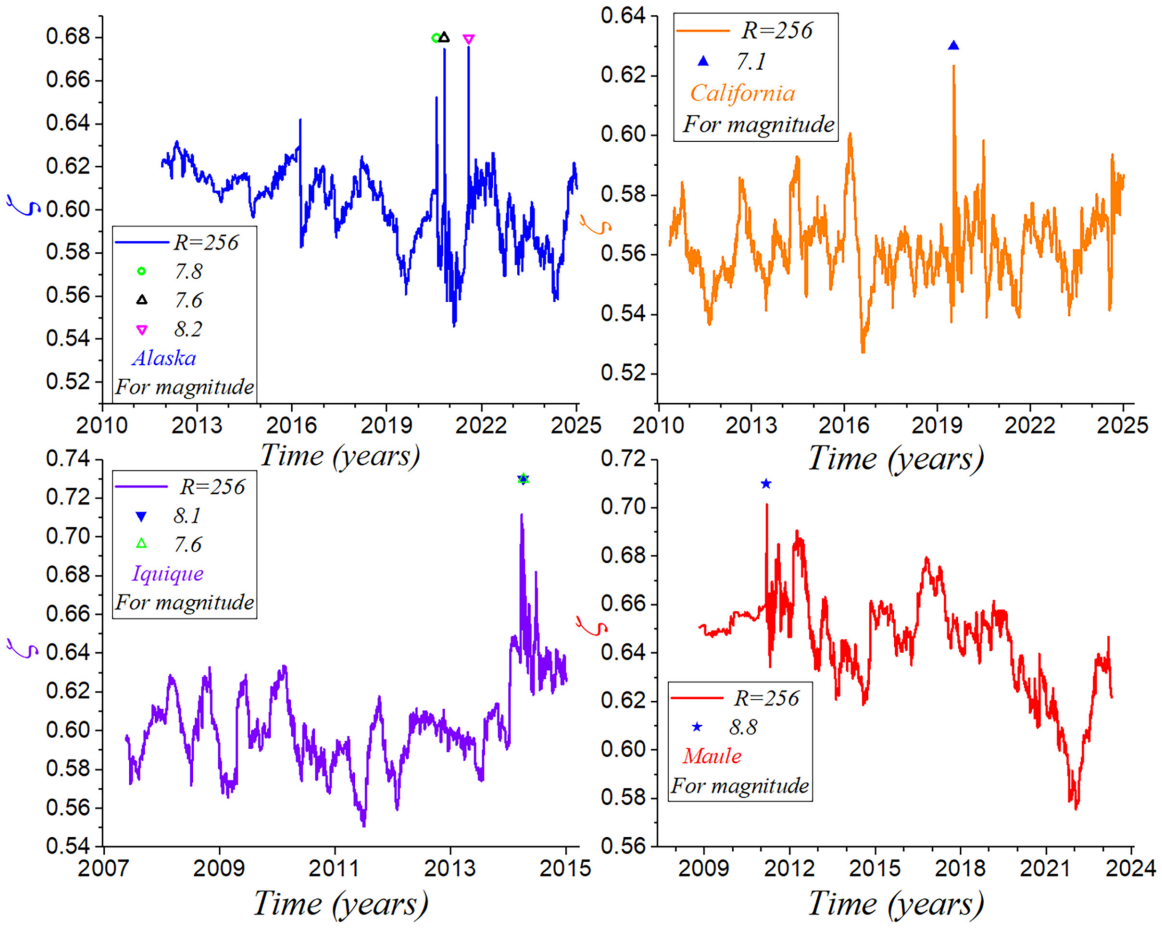


FIG. 5. Mutability on magnitude for the four seismic sequences corresponding to the four regions: Alaska, California, Iquique, and Maule.

We switch now to the diversity curves for the same previous data. Figure 7 presents the dynamical diversity δ with windows of 256 consecutive events, as in previous plots. The major earthquakes appear as upward needles at the corresponding time. All curves display texture, but some noise is evident. Alaska and Iquique showed lower values of δ years or months before the large earthquake. Nothing of this sort is to be found for California and it is impossible for Maule because of the lack of prior data.

Figure 8 presents the application of diversity to the interval sequences using time windows comprising 256 events, where the largest seisms produce clear, narrow needles. This visualization reveals other important seisms in the sequences, such as the 2016 Alaska earthquake, the 2020 and 2024 California earthquakes, and the 2010 Iquique earthquake. Actually, scrutiny of the data allows us to interpret broad minima as possible swarms of intermediate seisms.

VI. CONCLUSIONS

Intervals τ between successive seisms within a geographical region offer an alternative and complementary information to what magnitudes M can offer. As M gets monotonically smaller, τ gets larger. This agrees with the subduction model: as plates collide or stick, the slower sliding mechanism increases the time between successive earthquakes.

The four geographical regions rendered Gutenberg-Richter linear decays over five or six orders of magnitude, thus allowing for statistical treatments. The b values increase in the following order: Alaska (0.655), Iquique (0.711), Maule (0.787), and California (0.864). This shows an increasing correlation among earthquakes from Alaska to California; however, the Maule case might change if the catalog included a more complete set of foreshock records.

To avoid comparing direct intervals with a logarithm-defined parameter like magnitude, we defined latency as the logarithm of τ. Then the dynamical comparison between magnitude and latency provided a very interesting result: these magnitudes vary synchronically but in opposite senses. Thus, as average values of the magnitude increase for a large earthquake, the average value of the latency decreases. This feature provides a very graphical picture of the seismic dynamics. Interestingly, the latency curves present more details or texture than the corresponding magnitude curves.

Dynamical mutability curves on the magnitude series present sharp maxima at the time of the large earthquakes. Oscillatory decays follow them during the aftershock regimes. Periods with several moderate seisms (eventually swarms) appear as broad, small maxima. A search for premonitory signs provides no clear findings. We could consider the absolute minima months or years before large earthquakes as a possible warning in some cases. However, this is far from being a precursor and this subject needs further investigation

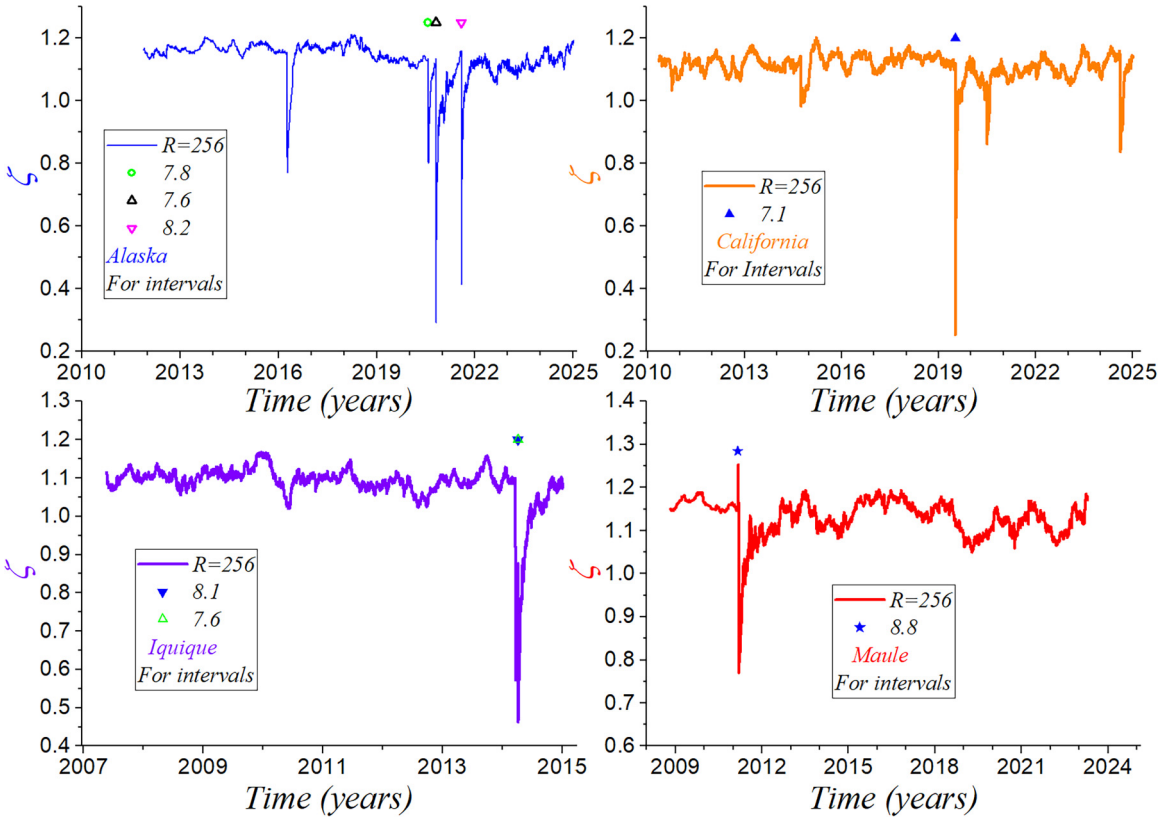


FIG. 6. Mutability on intervals for the four seismic sequences corresponding to the five regions: Alaska, California, Iquique, and Maule.

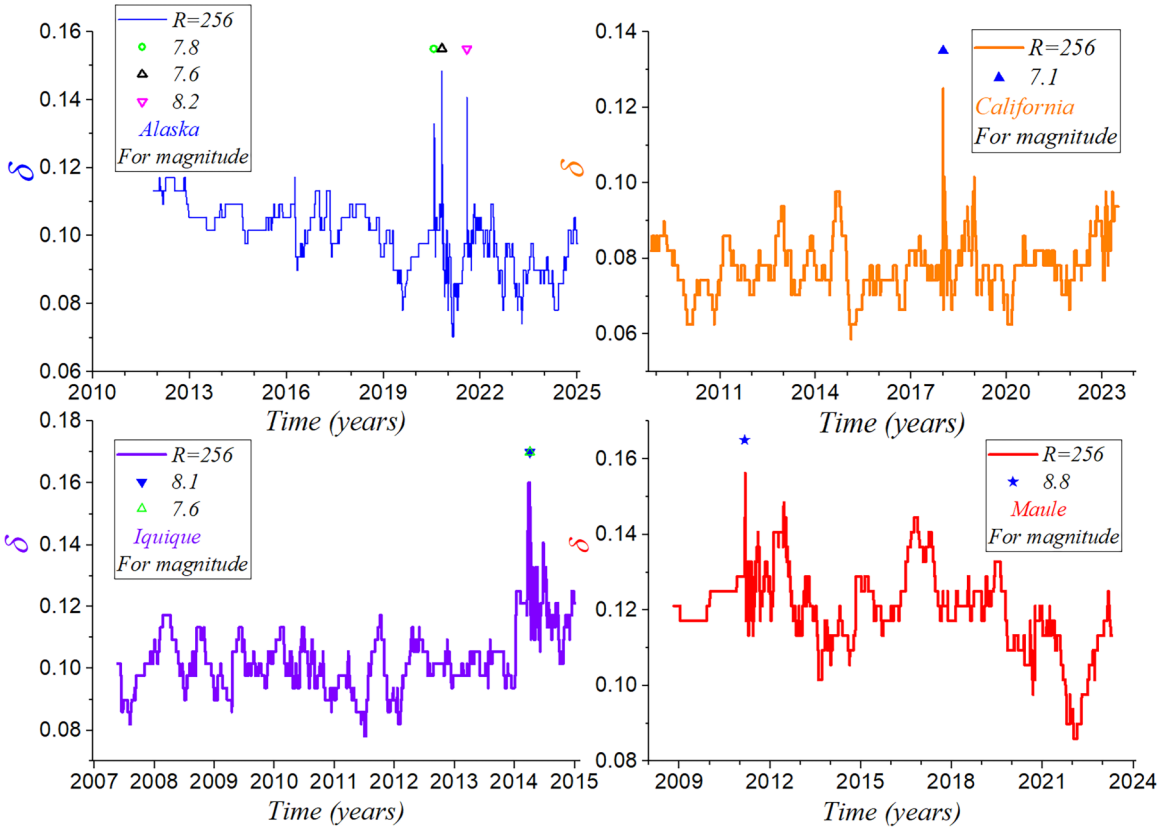


FIG. 7. Diversity on magnitude for the four seismic sequences corresponding to the four regions: Alaska, California, Iquique, and Maule. The time of the main earthquakes is indicated by symbols defined in the insets.

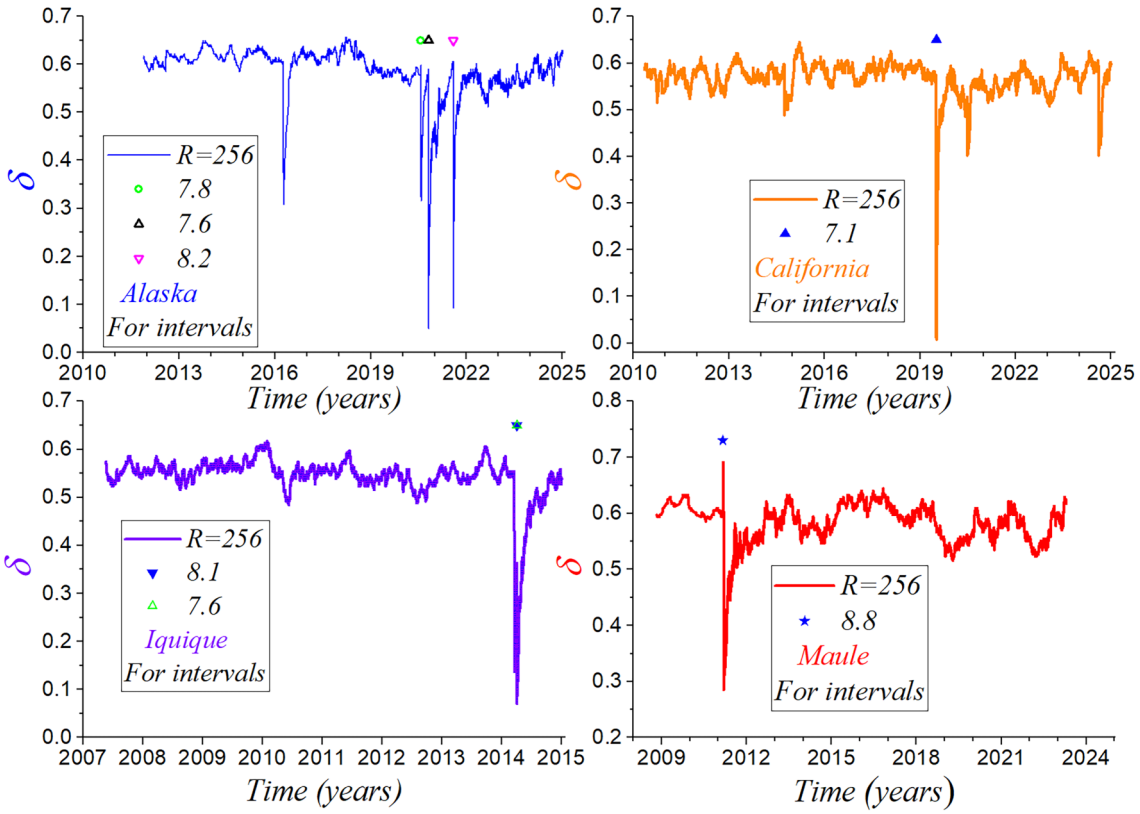


FIG. 8. Diversity on intervals for the four seismic sequences corresponding to the four regions: Alaska, California, Iquique, and Maule. The time of the main earthquakes is indicated by symbols defined in the insets.

in different geographical areas. The Maule region does not allow for this detailed analysis because of catalog limitations.

The dynamical mutability curves for intervals confirm previous features. Large earthquakes produce sharp, deep minima. However, even seismic events of magnitude over 5.0 show moderate sharp minima. Here, the aftershock regimes produce oscillatory increases of mutability. Premonitory signs are even more difficult to find in the case of intervals.

Diversity on magnitudes confirms results obtained by mutability, except that curves look discontinuous because diversity counts the number of different values within the R window, which is a discrete variable. Diversity curves present slightly more texture than mutability curves.

Diversity curves produce sharp, deep minima for intervals. Even moderate earthquakes and sequences of seisms (like swarms) are readily recognizable in the sequences. The aftershock activity shows clearly as oscillatory ascents approaching values close to those of previous major earthquakes. However, in none of the regions did the prior activity fully recover. With Iquique, the catalog does not allow this analysis.

Summarizing, the application of entropic analysis on intervals produces a clearer separation between large and moderate earthquakes, as well as characterizes sequences (swarms) of moderate earthquakes.

ACKNOWLEDGMENTS

E.E.V. acknowledges partial support from the Center for Nanoscience and Nanotechnology (CEDENNA, CIA 250002) (Chile) and Fondecyt (Chile) under Contract No. 1230055 and D.P. acknowledges support from Fondecyt (Chile) under Contract No. 1260714.

DATA AVAILABILITY

The data that support the findings of this article are openly available [10,11,25,26].

APPENDIX A

Shannon entropy follows the well-known relationship give by Eq. (11), where in our case the probabilities are obtained from a histogram originating in a data set. Such a histogram is independent of the sequence, namely, independent of the dynamics of the system.

Similarly, diversity is also independent of the dynamics since it only *counts* the original number of records ρ and the number of different records ρ^*. Then, Eq. (9) is invoked to calculate diversity. It has been shown that diversity is an entropic functional based on two Shannon entropies [48].

So although Shannon entropy and diversity can be formally related, they are calculated in completely different ways and reflect different sensitivities as it can be appreciated in Fig. 9.

On the contrary, mutability is based on the "maps" illustrated in the fourth and last columns of Table II. Such maps are clearly dependent on the way values repeat themselves in the sequence; hence they reflect the dynamics. Moreover, with these maps mutability can recover the original file which neither Shannon entropy nor diversity can do.

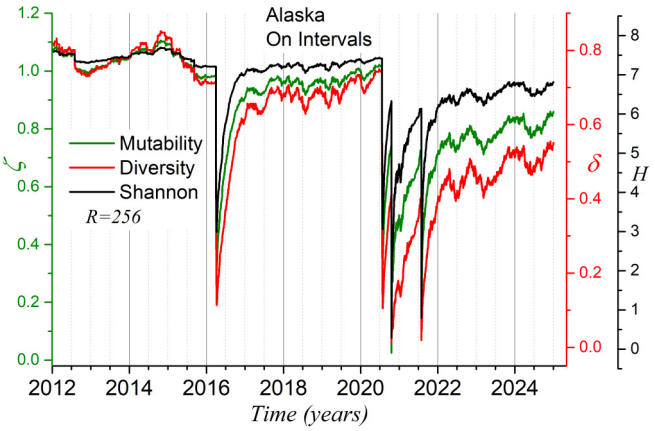


FIG. 9. Comparison of Shannon entropy, mutability, and diversity on intervals for the interval data of Alaska.

Figure 9 shows that the three functions recognize the major earthquakes of Alaska as downwards "needles." However, Shannon entropy presents less texture than the other two. Scales have been adjusted so the three curves present the same vertical maximum span. Prior to the earthquake of 2016 Shannon entropy is almost flat while diversity presents the largest oscillations. With the quake, diversity reaches the minimum in a more pronounced way. During the aftershock to the 2016 earthquake Shannon entropy recovers fast to the foreshock level, while the other two functions (especially diversity) take longer to recover, thus giving information on this process. Similar observations hold for the huge seismic activity of 2020, 2021, and the still lasting aftershock activity.

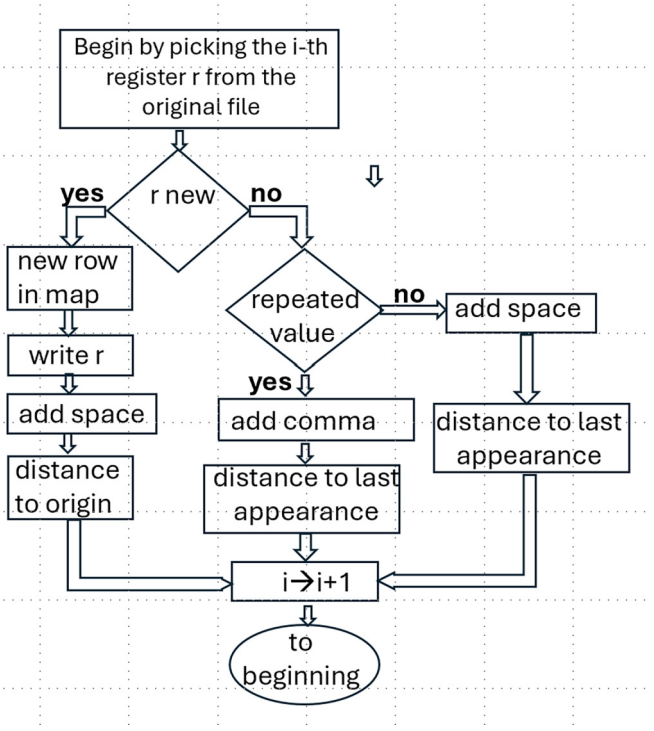


FIG. 10. One-loop flow chart to build the maps of Table II.

APPENDIX B

In the present appendix, we present the algorithm of information recognition WLZIP. This algorithm has been previously offered free of charge to the interested scientists and it is offered here once again by the authors. The package includes the code, a manual, and an example to facilitate its operation.

The purpose is to build the "maps" of the data as presented in Table II. We concentrate here on the magnitudes since this process can be easily extended to the intervals. Figure 10 presents the logic of WLZIP in the form of a flux diagram. The starting point is the original file F with the R equivalent measurements. It is important that all records here possess the same number of digits, writing zeros in all possible empty spaces. A new file G is created with one row for each different value in F. The row is initiated with the measured value; after a space we will have the position indices for this value in the original file as described in the flux diagram.

APPENDIX C

In this appendix, we test the sensitivity of mutability for both magnitudes with the number R of consecutive events. We concentrate here on $R = 128$ and $R = 256$ (which was used in all previous figures). A more complete discussion on this subject can be found in Pasten *et al.* [39]. Figure 11 shows Shannon entropy and mutability for the data of Alaska with just one difference: the size of the number of consecutive events used to calculate these functions. Scales have been adjusted as to give the same vertical span for better comparison. Both time windows give similar description; however, there are the following differences. (i) Curves are noisier (frequent oscillations) for $R = 128$. Actually, this is even more pronounced for $R = 64$ and lower (not shown). (ii) Contrasts between maxima and minima are better appreciated for $R = 256$, especially for mutability. (iii) Although increasing R to 512 increases the advantage of larger R values (not shown here), the time delay to gather the R events keeps increasing, needing years during the foreshock regime. So we settled for $R = 256$ as a compromise between contrast in the curves and recent information.

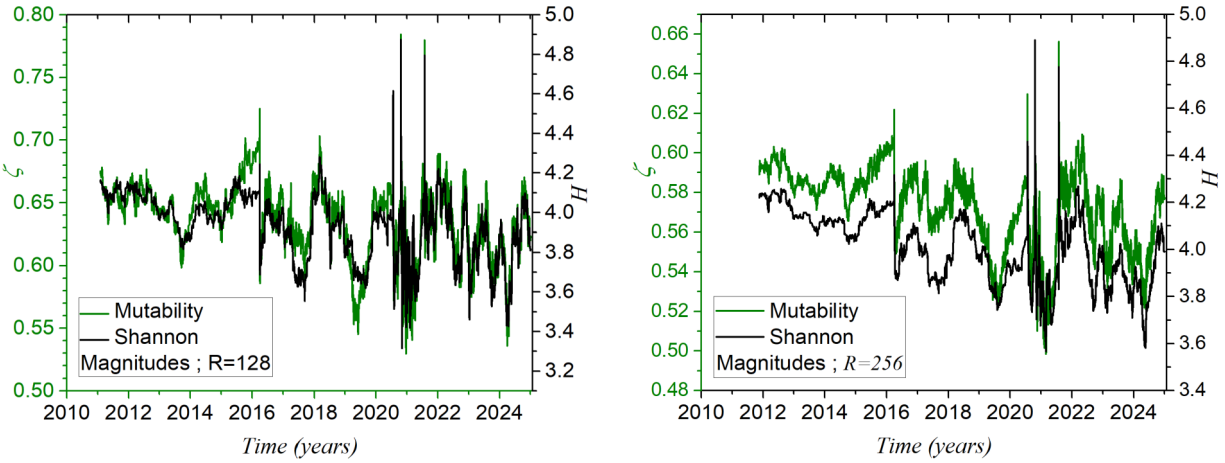


FIG. 11. Shannon entropy and mutability for the complete Alaska data using windows of 128 (left) and 256 (right) consecutive overlapping seisms.

[1] L. Telesca and C.-C. Chen, Nonextensive analysis of crustal seismicity in Taiwan, Nat. Hazards Earth Syst. Sci. **10**, 1293 (2010).

[2] L. Telesca, Tsallis-based nonextensive analysis of the Southern California seismicity, Entropy **13**, 1267 (2011).

[3] L. Telesca, Maximum likelihood estimation of the nonextensive parameters of the earthquake cumulative magnitude distribution, Bull. Seismol. Soc. Am. **102**, 886 (2012).

[4] N. V. Sarlis, E. S. Skordas, and P. A. Varotsos, Nonextensivity and natural time: The case of seismicity, Phys. Rev. E **82**, 021110 (2010).

[5] F. Vallianatos, G. Michas, and G. Papadakis, A description of seismicity based on non-extensive statistical physics: A review, in *Earthquakes and their Impact on Society*, edited by S. D'Amico (Springer Natural Hazards, Cham, 2015), p. 1.

[6] E. E. Vogel, F. G. Brevis, D. Pastén, V. Muñoz, R. A. Miranda, and A. C.-L. Chian, Measuring the seismic risk along the Nazca–South American subduction front: Shannon entropy and mutability, Nat. Hazards Earth Syst. Sci. **20**, 2943 (2020).

[7] A. Posadas, J. Morales, and A. Posadas, Earthquakes and entropy: Characterization of occurrence of earthquakes in southern Spain and Alboran Sea, Chaos **31**, 043124 (2021).

[8] A. Posadas, J. Morales, J. Ibáñez, and A. Posadas, Shaking earth: Non-linear seismic processes and the second law of thermodynamics: A case study from Canterbury (New Zealand) earthquakes, Chaos Solitons Fractals **151**, 111243 (2022).

[9] A. Posadas, D. Pasten, E. E. Vogel, and G. Saravia, Earthquake hazard characterization by using entropy: Application to northern Chilean earthquakes, Nat. Hazards Earth Syst. Sci. **23**, 1911 (2023).

[10] SSNMX, Servicio Sismológico Nacional de México, 2025.

[11] USGS, United States geological service, 2025.

[12] N. N. Biswas, J. Pujol, G. Tytgat, and K. Dean, Synthesis of seismicity studies for western Alaska, Tectonophysics **131**, 369 (1986).

[13] D. I. Doser and H. Rodriguez, A seismotectonic study of the southeastern Alaska region, Tectonophysics **497**, 105 (2011).

[14] R. Martin-Short, R. Allen, I. D. Bastow, R. W. Porritt, and M. S. Miller, Seismic imaging of the Alaska subduction zone: Implications for slab geometry and volcanism, Geochem., Geophys., Geosyst. **19**, 4541 (2018).

[15] K. Smith and C. Tape, Seismic Noise in Central Alaska and Influences From Rivers, Wind, and Sedimentary Basins, J. Geophys. Res.: Solid Earth **124**, 11678 (2019).

[16] K. A. Daly, G. A. Abers, M. E. Mann, S. Roecker, and D. H. Christensen, Subduction of an oceanic plateau across Southcentral Alaska: High-resolution seismicity, J. Geophys. Res.: Solid Earth **126**, e2021JB022809 (2021).

[17] R. Qu, Y. Ji, W. Zhu, Y. Zhao, and Y. Zhu, Fast and slow earthquakes in Alaska: Implications from a three-dimensional thermal regime and slab metamorphism, Appl. Sci. **12**, 11139 (2022).

[18] M. C. Arango, F. O. Strasser, J. J. Bommer, D. A. Hernández, and J. M. Cepeda, A strong-motion database from the Central American subduction zone, J. Seismol. **15**, 261 (2011).

[19] M. Arroyo-Solórzano and L. Linkimer, Spatial variability of the b-value and seismic potential in Costa Rica, Tectonophysics **814**, 228951 (2021).

[20] C. Gamboa-Canté, M. Arroyo-Solórzano, B. Benito, J. Aguilar, I. G. Arroyo, E. Camacho-Astigarrabia, D. Castro, O. Flores, L. Linkimer, M. G. Marroquin, L. Mixco-Durán, W. Strauch, E. Talavera, G. Valle, and R. Yani-Quiyuch, Seismicity in Central America (1520–2020) and Earthquake catalog compilation for seismic hazard assessments, Bull. Earthquake Eng. **22**, 7201 (2024).

[21] M. Métois, A. Socquet, C. Vigny, D. Carrizo, S. Peyrat, A. Delorme, E. Maureira, C. Valderas-Bermejo, and I. Ortega, Revisiting the North Chile seismic gap segmentation using GPS-derived interseismic coupling, Geophys. J. Int. **194**, 1283 (2013).

[22] M. Métois, C. Vigny, and A. Socquet, Interseismic coupling, megathrust earthquakes and seismic swarms along the Chilean subduction zone (38°–18°), Pure Appl. Geophys. **173**, 1431 (2016).

[23] B. Schurr, G. Asch, S. Hainzl, J. Bedford, A. Hoechner, M. Palo, R. Wang, M. Moreno, M. Bartsch, Y. Zhang, O. Oncken, F. Tilmann, T. Dahm, P. Victor, S. Barrientos, and J.-P. Vilotte,

Gradual unlocking of plate boundary controlled initiation of the 2014 Iquique earthquake, Nature (London) **512**, 299 (2014).
[24] C. Sippl, B. Schurr, T. John, and S. Hainzl, Filling the gap in a double seismic zone: Intraslab seismicity in northern Chile, Lithos **346-347**, 105155 (2019).
[25] IPOC, doi.org/10.1002/2017jb015384, 2020.
[26] U. de Chile, 2013: Red Sismologica Nacional. International Federation of Digital Seismograph Networks. Other/Seismic Network. 10.7914/SN/C1, https://doi.org/10.7914/sn/c1.
[27] H. Goldstein, C. Poole, and J. Safko, *Classical Mechanics*, 3rd ed. (Pearson, London, 2013).
[28] N. Zettili, *Quantum Mechanics: Concepts and Applications*, 3rd ed. (Wiley, New York, 2022).
[29] O. Sotolongo-Costa and A. Posadas, Fragment-asperity interaction model for earthquakes, Phys. Rev. Lett. **92**, 048501 (2004).
[30] R. Silva, G. S. França, C. S. Vilar, and J. S. Alcaniz, Nonextensive models for earthquakes, Phys. Rev. E **73**, 026102 (2006).
[31] A. H. Darooneh and A. Mehri, A nonextensive modification of the Gutenberg–Richter law: q-stretched exponential form, Physica A **389**, 509 (2010).
[32] S. M. Valverde-Esparza, A. Ramírez-Rojas, E. L. Flores-Márquez, and L. Telesca, Non-extensivity analysis of seismicity within four subduction regions in Mexico, Acta Geophys. **60**, 833 (2012).
[33] P. Varotsos, N. Sarlis, E. Skordas, T. Nagao, and M. Kamogawa, Natural time analysis together with non-extensive statistical mechanics shorten the time window of the impending 2011 Tohoku $M9$ earthquake in Japan, Commun. Nonlinear Sci. Numer. Simul. **125**, 107370 (2023).
[34] P. A. Varotsos, N. V. Sarlis, E. S. Skordas, T. Nagao, M. Kamogawa, E. L. Flores-Márquez, A. Ramírez-Rojas, and J. Perez-Oregon, Improving the estimation of the occurrence time of an impending major earthquake using the entropy change of seismicity in natural time analysis, Geosciences **13**, 222 (2023).
[35] D. Schorlemmer, S. Wiemer, and M. Wyss, Variations in earthquake-size distribution across different stress regimes, Nature (London) **437**, 539 (2005).
[36] C. Shannon, A mathematical theory of communication, Bell Syst. Tech. J. **27**, 379 (1948).
[37] C. Shannon and W. Weaver, *The Mathematical Theory of Communication* (The Board of Trustees of the University of Illinois, Urbana-Champaign, 1949).
[38] E. Vogel, G. Saravia, and L. Cortez, Data compressor designed to improve recognition of magnetic phases, Physica A **391**, 1591 (2012).
[39] D. Pastén, E. E. Vogel, G. Saravia, and A. Posadas, Spatial, Temporal, and Dynamic Behavior of Different Entropies in Seismic Activity: The February 2023 Earthquakes in Türkiye and Syria, Entropy **27**, 462 (2025).
[40] D. Pasten, E. E. Vogel, G. Saravia, A. Posadas, and O. Sotolongo, Tsallis entropy and mutability to characterize seismic sequences: The case of 2007–2014 Northern Chile earthquakes, Entropy **25**, 1417 (2023).
[41] E. E. Vogel, D. Pastén, G. Saravia, M. Aguilera, and A. Posadas, 2021 Alaska earthquake: Entropy approach to its precursors and aftershock regimes, Nat. Hazards Earth Syst. Sci. **24**, 3895 (2024).
[42] E. Vogel and G. Saravia, Information theory applied to econophysics: Stock market behaviors, Eur. Phys. J. B **87**, 177 (2014).
[43] E. E. Vogel, G. Saravia, and A. J. Ramirez-Pastor, Phase transitions in a system of long rods on two-dimensional lattices by means of information theory, Phys. Rev. E **96**, 062133 (2017).
[44] E. E. Vogel, G. Saravia, D. Pastén, and V. Muñoz, Time-series analysis of earthquake sequences by means of information recognizer, Tectonophysics **712-713**, 723 (2017).
[45] O. Negrete, P. Vargas, F. Pena, G. Saravia, and E. Vogel, Entropy and mutability for the q-state clock model in small systems, Renewable Energy **20**, 933 (2018).
[46] E. Vogel, G. Saravia, S. Kobe, R. Schumann, and R. Schuster, A novel method to optimize electricity generation from wind energy, Renewable Energy **126**, 724 (2018).
[47] O. A. Negrete, P. Vargas, F. J. Peña, G. Saravia, and E. E. Vogel, Short-range Berezinskii-Kosterlitz-Thouless phase characterization for the q-state clock model, Entropy **23**, 1019 (2021).
[48] E. E. Vogel, C. Tsallis, and G. Saravia, Diversity as an entropic measure derived from entropic-like functionals, Phys. Rev. E **113**, 044127 (2026).